Biol. Cybern. 91, 188–202 (2004)
DOI 10.1007/s00422-004-0497-z

Biological Cybernetics

A model of cerebellum stabilized and scheduled hybrid long-loop control of upright balance

Sungho Jo, Steve G. Massaquoi

Department of Electrical Engineering and Computer Science (LIDS/CSAIL), MIT and MIT-Harvard HST NeuroEngineering Research Collaborative, 32 Vassar Street 32-206, Cambridge, MA 02139, USA

Received: 1 March 2004 / Accepted: 22 June 2004 / Published online: 14 September 2004

Abstract. A recurrent integrator proportional integral derivative (PID) model that has been used to account for cerebrocerebellar stabilization and scaling of transcortical proprioceptive feedback in the control of horizontal planar arm movements has been augmented with long-loop force feedback and gainscheduling to describe the control of human upright balance. The cerebellar component of the controller is represented by two sets of gains that each provide linear scaling of same-joint and interjoint long-loop stretch responses between ankle, knee, and hip. The cerebral component of the model includes a single set of same-joint linear force feedback gains. Responses to platform translations of a three-segment body model operating under this hybrid proprioception and force-based long-loop control were simulated. With low-velocity platform disturbances, "ankle-strategy"-type postural recovery kinematics and electromyogram (EMG) patterns were generated using the first set of cerebeller control gains. With faster disturbances, balance was maintained by including the second set of gains cerebellar control gains that yielded "mixed ankle-hip strategy"-type kinematics and EMG patterns. The addition of small amounts of simulated muscular coactivation improved the fit to certain human datasets. It is proposed that the cerebellum switches control gainsets as a function of sensed body kinematic state. Reduction of cerebellar gains with a compensatory increase in muscular stiffness yielded posture recovery with abnormal motions consistent with those found in cerebellar disease. The model demonstrates that stabilized hybrid long-loop feedback with scheduling of linear gains may afford realistic balance control in the absence of explicit internal dynamics models and suggests that the cerebellum and cerebral cortex may contribute to balance control by such a mechanism.

1 Introduction

Engineering models have been developed that effectively describe aspects of human balance (Kuo 1995), locomotor (Ogihara and Yanazaki 2001), and jumping control (Spagele et al. 1999). However, few have made specific proposals for how this may be implemented by the central nervous system (CNS). In particular, the performance of CNS feedback control systems must be evaluated carefully given that transcortical round trip (long-loop) signal transmission delays to and from trunk and ankle are on the order of 60–80 ms, respectively, and additional phase lags occur due to neuromuscular excitation–activation coupling (Fuglevand and Winter 1993). Especially the latter have been frequently neglected, which leaves in question some conclusions regarding the stability of some balance models. The issue of delay management in motor physiological feedback control has been specifically addressed by other investigators. Models differ with respect to whether they propose (Uno et al. 1989; Miall et al. 1993; Paulin 1993b; Wolpert et al. 1998) or do not propose (Lacquaniti and Soechting 1986; Massaquoi and Slotine 1996; Kettner et al. 1997) that the CNS incorporates internal dynamics models to achieve sufficient signal prediction for stabilization of long-loop responses. In a number of these descriptions, the function of the cerebellum is represented prominently because of its established importance in both movement control and postural stabilization (Diener and Dichgans 1992; Thach et al. 1992b; Massaquoi and Hallett 1997). Internal-dynamics-model-based approaches to physiological state estimation/prediction, including those based on Kalman filtering (Kuo 1995; Paulin 1997), Smith predictors (Miall et al. 1993), or other schemes (Uno et al. 1989; Kettner et al. 1997), are clearly powerful and well motivated from an engineering viewpoint. Yet, while the CNS is presumably sufficiently complex to include circuits that could match the dynamic order and nonlinearity of the body itself, there is no specific evidence that such mechanisms are actually active. Therefore, the question of whether the brain uses computational schemes that are simpler and/or more efficient in terms of neuronal processing remains an open one. For example, Ayaso et al. (2002) have demonstrated that effective inverse kinematic modeling may be achieved implicitly using relatively coarsely specified gain settings within feedback control loops. Similarly, "direct"

Correspondence to: S. Jo (e-mail: shjo@mit.edu)

control approaches (Goodwin and Sin 1984), including those linear schemes based on wave-variable processing (Massaquoi and Slotine 1996; Massaquoi 1999), or recurrent integrators (Massaquoi 1999), demonstrate that internal dynamics models are not necessary for stable delayed long-loop control.

The recurrent integrator proportional integral derivative (RIPID) model of cerebrocerebellar control (Massaquoi 1999) posits a particularly simple mechanism for stabilizing long-loop proprioceptive feedback loops to achieve arm posture and movement and postural control in the horizontal plane. Specifically, it proposes that corollary efference-copy discharge (Hore and Vilis 1984) transmitted via a cerebellar integrator returns to the cerebral cortex to afford effective differentiation and thereby phase lead critical for long-loop stability. Once stabilized, linear scaling of same-joint and interjoint feedback responses by linear gains is sufficient to manage plant dynamics. A number of features of human arm control, both for intact and compromised cerebellar function, appear to be well described by the model. However, it is not clear that this type of mechanism would be able to properly address the nonlinear and inherently unstable dynamics of an upright multisegment plant. An initial application of the RIPID model to controlling the upright posture of a simple three-segment body model that included lumped nonlinear but not activation-dependent joint stiffness and viscosity was only partially successful. It was able to supplement comparatively low (<100 Nm/rad) ankle muscular stiffness to reproduce low-velocity body balancing that depends primarily upon control of ankle torques ("ankle strategy", Horak and Nashner 1986; Nashner and McCollum 1985). In this regard, the model afforded a neuroanatomically plausible implementation of PID balance control that had been posited previously by Johansson et al. (1988) and Peterka (2001, 2003). However, for stronger disturbances that called for coordinated ankle and hip motion ("mixed ankle-hip strategy", Horak and Nashner 1986; Nashner and McCollum 1985), the RIPID model was unable to reproduce human balancing kinematics unless the cerebellar gains were switched during motion. Three sets of linear gains, a base set for quiet standing, a "catching" set, and a "recovery" set, were ultimately found to be sufficient to reproduce characteristic human kinematics following platform translations over a large range of velocities (Jo 2002). To accomplish this, it was postulated that cerebellar control switched between the three gain-sets on the basis of sensed body kinematic state. While the approach appeared promising, it was found (unpublished) that when using more realistic muscle models, the switching required for comparable performance became considerably more complicated.

Another important approach to antigravity and balance control appears to be the use of force feedback. Positive force feedback has been shown to be valuable in managing ground impact during robotic locomotion (Song et al. 1999). In this case, it can compensate strongly for declining mechanical advantage as the body or joint bends under gravity. In relation to stance, Peterka (2003) has pointed out that, at least for gentle ($\leq 1^\circ$ excursion) induced body sway about the ankle, positive force feedback added to PID control appears to provide low-frequency phase advance that contributes to stability. For the low-frequency (<2 Hz) movements studied, additional mechanisms for long-loop delay compensation were not required. There is no indication, however, that the addition of positive force feedback to simple PID control is itself sufficient to stabilize stance against large, rapid disturbances. On the other hand, negative force feedback may have a role in this situation. Preliminary simulations subjecting the switched RIPID model with activation-dependent muscular stiffness to strong disturbances demonstrated that it readily achieved upright posture but exhibited *excessively rapid* return to vertical. This inappropriately large effective stiffness about vertical indicated that the addition of negative rather than positive force feedback might provide more realistic responses. The hybrid force feedback RIPID (FRIPID) model is designed to agree with accepted or highly plausible motor system neuroanatomy and has been assessed with respect to its ability to reproduce human kinematics and EMG patterns in the context of intact and compromised cerebellar function. It was found that the incorporation of negative force feedback enables the proprioception-based switched RIPID control model to reproduce human behavior across a range of disturbance intensities using a simpler kinematic state-based gainscheduling scheme than was possible before. The model's qualitative reproduction of balance dysfunction in cerebellar disease supports its formulation of the role of cerebrocerebellar circuitry in balance control.

2 Methods

2.1 Musculoskeletal plant model

A three-segment kinematic chain with pivot joints representing the ankle, knee, and hip was used to represent human rigid body dynamics in the sagittal plane (Fig. 1). Positive angular motion was consistent with anatomical flexion at the hip, knee, and dorsiflexion at the ankle. The feet were assumed to be always in flat stable contact with the ground (platform). After computation of motion, it was verified that ankle torques and center-of-mass location would not have caused heel lift or loss of balance. The body model's dynamics in response to applied total muscular and disturbance torques applied to the joints, $\boldsymbol{\tau}_{\mathrm{M}}(\boldsymbol{\Theta}, \dot{\boldsymbol{\Theta}}, \mathbf{u}_{\boldsymbol{\theta}})$ and $\boldsymbol{\tau}_{\mathrm{D}}(\ddot{D}, \boldsymbol{\Theta})$, respectively, is given by:

$$\mathbf{H}(\boldsymbol{\Theta})\ddot{\boldsymbol{\Theta}} + \mathbf{C}(\boldsymbol{\Theta}, \dot{\boldsymbol{\Theta}}) = \boldsymbol{\tau}_{\mathrm{M}}(\boldsymbol{\Theta}, \dot{\boldsymbol{\Theta}}, \mathbf{u}_{\boldsymbol{\theta}}) + \boldsymbol{\tau}_{\mathrm{D}}(\ddot{D}, \boldsymbol{\Theta}) + \mathbf{G}(\boldsymbol{\Theta}), \quad (1)$$

where $\boldsymbol{\Theta} = [\theta_1 \quad \theta_2 \quad \theta_3]^{\mathrm{T}}$, $\dot{\boldsymbol{\Theta}} = \left[\dot{\theta}_1 \quad \dot{\theta}_2 \quad \dot{\theta}_3\right]^{\mathrm{T}}$, and $\mathbf{u}_{\boldsymbol{\theta}}$ is the 3×1 central command vector from brain. $\mathbf{H}(\boldsymbol{\Theta})$ is the 3×3 symmetric configuration-dependent body inertia matrix, $\mathbf{C}(\boldsymbol{\Theta}, \dot{\boldsymbol{\Theta}})$ is the 3×3 matrix related to centrifugal and Coriolis forces, $\mathbf{G}(\boldsymbol{\Theta})$ is the 3×3 gravitational effect matrix, and $\boldsymbol{\tau}_{\mathrm{D}}(\ddot{D}, \boldsymbol{\Theta})$ is the 3×1 vector related to external disturbance

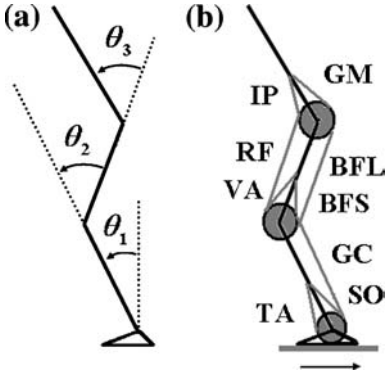

Fig. 1. **a** Body segment parameters and body configuration angle conventions: $\boldsymbol{\theta}_{\text{ankle}} = \boldsymbol{\theta}_1, \boldsymbol{\theta}_{\text{knee}} = -\boldsymbol{\theta}_2, \boldsymbol{\theta}_{\text{hip}} = \boldsymbol{\theta}_3$. **b** Muscle diagram: GM gluteus maximus, IP iliopsoas, BFL biceps femoris long, BFS biceps femoris short, RF rectus femoris, VA vastus intermedius, GC gastrocnemius, SO soleus, TA tibialis anterior

generated by backward platform acceleration ($\ddot{D}$). See appendix A for more detailed definitions.

Joint torque is determined by the total muscular force (passive + active) $\mathbf{F}(\mathbf{l}, \dot{\mathbf{l}}, \mathbf{u})$ and the moment arms of each muscle according to:

$$\boldsymbol{\tau}_{\text{M}}(\boldsymbol{\Theta}, \dot{\boldsymbol{\Theta}}, \mathbf{u}_\theta) = \mathbf{A}^{\text{T}}\mathbf{F}(\mathbf{l}, \dot{\mathbf{l}}, \mathbf{u}) \tag{2}$$

$$\mathbf{A}^{\text{T}} = \begin{bmatrix} -a_1 & 0 & 0 & 0 & -a_5 & a_6 & 0 & 0 & a_9^{\text{a}} \\ 0 & 0 & a_3 & -a_4 & 0 & 0 & a_7^{\text{k}} & -a_8^{\text{k}} & -a_9^{\text{k}} \\ 0 & a_2 & 0 & 0 & 0 & 0 & -a_7^{\text{h}} & a_8^{\text{h}} & 0 \end{bmatrix} \tag{3}$$

where a_i is the estimated average moment arm of the ith muscle in Table 1. This formulation substantially follows that employed by Katayama and Kawato (1993) except that muscles are activated simply in relation to intended joint control (Equation 8) and muscles undergo a simple step change in stiffness with activation. For biarticular muscles, superscripts h, k, and a represent moment arms at, respectively, the hip, knee, and ankle. Flexor moment arms are negative, reflecting the relationship between length change and direction of rotation.

Passive muscular force is expressed by:

$$\mathbf{F}_{\text{p}} = [\mathbf{K}_{\text{p}}(\mathbf{l}_{\text{eq}} - \mathbf{l}) - \mathbf{B}_{\text{p}}\dot{\mathbf{l}}]_+ , \tag{4}$$

where $[x]_+ = \begin{cases} x & x > 0 \\ 0 & x \le 0 \end{cases}$ F_{p} is passive tension, $\mathbf{K}_{\text{p}}, \mathbf{B}_{\text{p}}$ are passive muscle stiffness and viscosity, $\mathbf{l}_{\text{eq}}$ is muscle length at equilibrium, and l is actual muscle length.

Active muscular force as a function of neural input to each muscle ($\mathbf{u}$) is represented by:

$$\mathbf{F}_{\text{a}} = [\mathbf{K}_{\text{a}}\text{sgn}([\mathbf{l}(\mathbf{u}) - \mathbf{l}]_+)(\mathbf{l}(\mathbf{u}) - \mathbf{l}) - \mathbf{B}_{\text{a}}\text{sgn}([\mathbf{l}(\mathbf{u}) - \mathbf{l}]_+)\dot{\mathbf{l}}]_+ , \tag{5}$$

where $\mathbf{sgn}(x) = \begin{cases} 1 & x > 0 \\ 0 & x = 0 \\ -1 & x < 0 \end{cases}$ $\mathbf{F}_{\text{a}}$ is active tension, $\mathbf{K}_{\text{a}}, \mathbf{B}_{\text{a}}$ active are flexor muscle stiffness and viscosity, $\mathbf{l}_{\text{eq}}$ is muscle length at equilibrium, $\mathbf{l}$ is actual muscle length $\mathbf{l}(\mathbf{u}) = \mathbf{l}_{\text{eq}} + \alpha\mathbf{u}$, where α is constant (activation-to-length gain), and $\mathbf{u}$ is neural input.

When both passive and active tensions are applied together,

$$\mathbf{F}(\mathbf{l}, \dot{\mathbf{l}}, \mathbf{u}) = \mathbf{F}_{\text{p}}(\mathbf{l}, \dot{\mathbf{l}}) + \mathbf{F}_{\text{a}}(\mathbf{l}, \dot{\mathbf{l}}, \mathbf{u}) , \tag{6}$$

$$\mathbf{l} = \mathbf{l}_{\text{eq}} + \mathbf{A}(\boldsymbol{\Theta} - \boldsymbol{\Theta}_{\text{eq}}) , \tag{7}$$

$$\mathbf{u} = \mathbf{A}\mathbf{u}_\theta \tag{8}$$

(α is set at 1 for simulation).

The activation of muscle force by neural input occurs according to low-pass dynamics that can be approximated by:

$$EC(s) = \frac{\rho^2}{(s+\rho)^2} \quad \rho = 30\,\text{rad/s} \quad \text{(Fuglevand and Winter 1993)} . \tag{9}$$

The model views the similarly acting muscles of the trunk and legs as operating together as functional groups of uni- and biarticular flexors and extensors as shown in Fig. 1b. Assuming that stiffness is proportional to the physiological cross-sectional area (PCA) (Brand et al. 1986), the relative muscle stiffness scaling is given based on morphmetric data in Table 1. The effective preset (i.e., before reflex neural activation) rotational stiffness of the ankle during standing is about 90 Nm/rad (Fujita and Sato 1998). This value was used to determine the absolute passive stiffness of each muscle given its relative scaling.

The muscle viscosity was set at one tenth the muscle stiffness as has been done in arm modeling (Flash 1987). The passive stiffness is assumed to include the action of segmental reflexes as in the "lambda model" of Feldman (Feldman 1986). The dynamics of series elasticity, filtering action of spindles, segmental proprioceptive and force feedback, and spinal processing by alpha motorneuron–Renshaw cell networks were not modeled explicitly, although it is likely that these could improve the accuracy of the simulations (Winters 1995). It was not felt that these features would bear significantly upon the question of FRIPID control feasibility. Finally, it was assumed that muscular activation simply doubled the modest passive stiffness and viscosity of each muscle, which increases the damping ratio by 40%. This was considered based on human arm modeling where stiffness and damping ratio have been shown to increase up to 500 and 50%, respectively (Lacquaniti and Soechting 1986), with strong activation, and this was considered conservative leaving a larger portion of the control to the CNS model.

2.2 Neural control model

2.2.1 Cerebellar computation. Incorporating ideas from Oscarsson (1979), Ito (1984, 1997) proposed that cerebellar processing is performed by functional corticonuclear microcomplexes of various forms. Using this framework, it may be argued specifically that the cerebellum could afford proportional scaling, integration, and differentiation (Massaquoi 1999; Massaquoi and Topka 2002). Figure 2a indicates how proportional scaling, with or without approximate differentiation, could be implemented by a corticonuclear microcomplex in lateral cerebellum.The

Table 1. Length, moment arm, and physiological cross-sectional area (PCA) parameter values of muscles determined on the basis of Ogihara and Yamazaki (2001), Delp et al. (1999), and Winter (1990)

Muscle	Location	Length (m)	Moment arm (m)	PCA (cm^2)
Iliopsoas (IP)	Mono, hip flexor	0.35	0.002	17
Gluteus maximus (GM)	Mono, hip extensor	0.30	0.03	30.4
Rectus femoris (RF)	Bi, hip flexor, knee extensor	0.48	0.049 (h), 0.025 (k)	12.5
Biceps femoris long (BFL)	Bi, knee flexor, hip extensor	0.46	0.054 (h), 0.049 (k)	15.8
Vastus (VA)	Mono, knee extensor	0.26	0.04	30
Biceps femoris short (BFS)	Mono, knee flexor	0.29	0.049	6.8
Tibialis anterior (TA)	Mono, ankle dorsiflexor	0.30	0.023	9.1
Gastrocnemius (GC)	Bi, knee flexor, ankle plantarflexor	0.56	0.050 (k), 0.040 (a)	30
Soleus (SO)	Mono, ankle plantarflexor	0.35	0.036	58

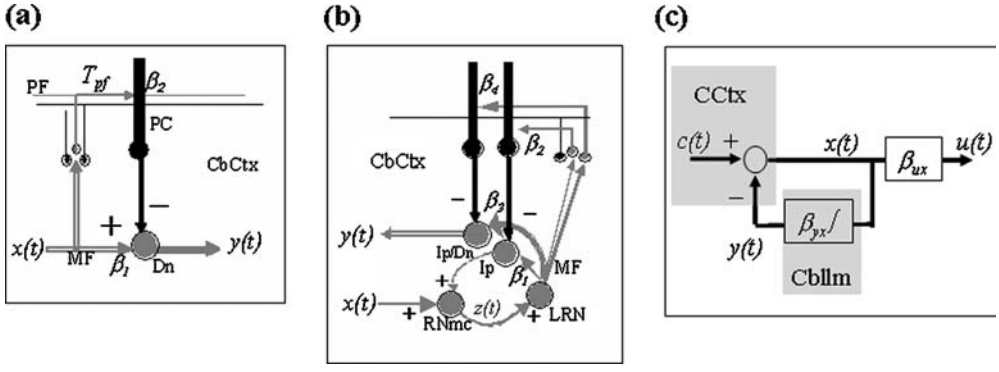

Fig. 2a–c. Neural computation in cerebellar corticonuclear complex (**a**) differentiation, (**b**) integration band-limited differentiation

input signal $x(t)$ is conveyed by mossy fibers (MF) and the output signal $y(t)$ is transmitted from the dentate nucleus (Dn). A sidepath through the cerebellar cortex (CbCtx) contains a potentially significant time delay T_{pf} due to comparatively slowly conducting parallel fibers (PF) (Braitenberg 1967). Synaptic connection strengths between MF and dentate nuclear cells and between PF and Purkinje cells (PC) are represented as β_1 and β_2, respectively. The latter gain is generally considered to be adaptable (Ito 1984). The proposed input–output relationship is therefore $y(t) = \beta_1 x(t) - \beta_2 x(t - T_{pf})$, or $y(t) = \beta_x x(t) - \beta_2(x(t) - x(t - T_{pf}))$. Therefore, $y(t) \approx \beta_x x(t) + T_{pf}\beta_2 \mathrm{d}x(t)/\mathrm{d}t$, where $\beta_x = \beta_1 - \beta_2$, and output signal scaling and character can be modified by adaptation of β_2. When $\beta_1 \approx \beta_2$ and T_{pf} is nontrivial, output is proportional to an approximate derivative of the input. Otherwise, the output consists of a signal proportional to input, possibly together with an additional derivative term.

Figure 2b suggests that integration may be afforded by interaction between cerebellar corticonuclear complexes in the medial cerebellum together and certain precerebellar nuclei. Input $x(t)$ is transmitted by cells in magnocellular red nucleus (RNmc) and lateral reticular nucleus (LRN) to interpositus nuclear cells (Ip) (Allen and Tsukahara 1974). RNmc units are modeled as a leaky integrator with nontrivial time constant τ because of their large size. In this case, $\mathrm{d}z(t)/\mathrm{d}t = x(t) + (\beta_1 - \beta_2)z(t) - (1/\tau)z(t)$. For $(\beta_1 - \beta_2) \approx (1/\tau)$, we have $\mathrm{d}z(t)/\mathrm{d}t \approx x(t)$ and hence $z(t) \approx \int x(t)\mathrm{d}t$. This proposed adaptive (via changes in β_2) cancellation of integrator leak is analogous to that proposed for eye control (Leigh and Zee 1991). Therefore, $y(t) \approx \beta_3 z(t) - \beta_4 z(t - T_{pf})$. By the analysis in Fig. 2a, $y(t) \approx \beta_x \int x(t)\mathrm{d}t + T_{pf}\beta_3 x(t)$, where $\beta_x = \beta_3 - \beta_4$. The output is therefore approximately a scaled version of the integral of the input and/or a term proportional to the input if T_{pf} is not negligible.

Finally, Fig. 2c depicts how a band-limited differentiator may be implemented using the cerebellar integrator in Fig. 2b scaled by an arbitrary gain $\beta_{yx} = \beta_x = \beta_3 - \beta_4$ and connected in negative feedback configuration with respect to the cerebral cortex CCtx. Here, $c(t)$ is a high-level command signal and the output is scaled by β_{ux} also possibly by cerebellar circuits. The net motor command is $u(t) = \beta_{ux}(c(t) - \beta_{yx} \int (u(t)/\beta_{ux})\mathrm{d}t)$. By differentiating and rearranging, $u(t) + (1/\beta_{yx})\mathrm{d}u(t)/\mathrm{d}t = (\beta_{ux}/\beta_{yx})\mathrm{d}c(t)\mathrm{d}t$. Because for any sinusoid, $\max_t |\mathrm{d}u(t)/\mathrm{d}t| = \omega \max_t |u(t)|$, the second term on the left can be neglected for signals having all frequency content $w \ll \beta_{yx}$. In this case, $u(t) \approx (\beta_{ux}/\beta_{yx})\mathrm{d}c(t)/\mathrm{d}t$, and the recurrent integrator provides effective differentiation.

It should be noted that in principle velocity information potentially available from muscle spindles could be used for the derivative component of control. In practice, however, this could be problematic. Spindle signals depend upon both muscle stretch and gamma biasing. Accurate computation of muscle stretch rate involves canceling the effect of bias rate of change, which is nontrivial because spindle response is not a simple function of bias input (Hasan 1983; Rosenthal et al. 1970). Moreover, arm control appears to benefit from double derivative control (Massaquoi 1999), which would be even

more difficult to extract from spindle information. RIPID models emphasize central differentiation. First, as argued above, this appears to be eminently feasible. Second, many phasic features of motor commands remain after peripheral deafferentation (Hallett et al. 1975), while instability consistent with loss of phase lead is prominent with cerebellar outflow lesions (Massaquoi 1999; Massaquoi and Topka 2002; Hore and Flament 1986). Third, central areas felt to receive spindle information show comparatively suppressed position information consistent with central differentiation (Hore et al. 1976). Still, the FRIPID model attempts to demonstrate that, for balance control, peripheral measurement of joint angular velocity is not necessary, rather than to insist that it does not occur.

2.2.2 Cerebrocerebellar long-loop feedback systems. The rotational stiffness of passive muscle at the ankle is not sufficient to maintain the body in upright balance. Based on a simple linear analysis about the vertical (unstable) equilibrium with knee assumed to be locked, the minimum effective stiffness needed at the ankle joint for static erect posture is about 700 Nm/rad (for a 70-kg individual with height of c.o.m =1 m). Therefore, some additional muscular activation is necessary. This may take the form of either feedforward coactivation of flexors and extensors around a joint to increase its effective stiffness and viscosity or neural feedback pathways. We seek a model that incorporates the minimum level of muscular coactivation consistent with observed behavior.

The hybrid force feedback RIPID (FRIPID) model is shown in Fig. 3. The model formally contains a vertical reference signal ($\mathbf{\Theta}_{\text{ref}}$) to acknowledge the fact that the CNS presumably can compute body orientation with respect to vertical (Peterka 2003). As even subjects with significant vestibular dysfunction may be able to balance (Nashner et al. 1982), the orienting mechanism can utilize multisensory inputs. For simple upright balancing on a horizontal platform, $\mathbf{\Theta}_{\text{ref}}$ and $\boldsymbol{\tau}_{\text{ref}}$ can be set to zero. We propose that the linear PID processing shown in Fig. 2 can be extended directly to three-joint control such that the cerebellar output is given by:

$$\mathbf{u}_{\text{cb}}(i) = \sum_{j=1,2,3} \mathbf{G}_{\text{b}}^{(m)}(i,j)\dot{\mathbf{x}}_{\text{cb}}(j) + \sum_{j=1,2,3} \mathbf{G}_{\text{k}}^{(m)}(i,j)\mathbf{x}_{\text{cb}}(j) + \sum_{j=1,2,3} \mathbf{I}_{1}^{(m)}(i,j) \int \mathbf{x}_{\text{cb}}(j), \tag{10}$$

where $\int \mathbf{x} = \int_0^{\text{t}} \mathbf{x}(\boldsymbol{\tau})\text{d}\boldsymbol{\tau}$.

Here $\mathbf{G}_{\text{k}}^{(m)}$, $\mathbf{G}_{\text{b}}^{(m)}$, and $\mathbf{I}_{1}^{(m)}$ are 3×3 matrices that belong to gainset $m = 1, 2$ as described in the next section. Therefore, (10) represents linear control for any m and piecewise linear control overall. Empirically, differentiation of $\mathbf{x}_{\text{cb}}$ was found to be unnecessary for balance simulations. Therefore, the elements of $\mathbf{G}_{\text{b}}^{(m)}$ were set to zero.

As in the basic RIPID model (Massaquoi 1999), the 3×3 matrices I_{a} and I_{τ} are proposed to represent scaling of signals related to hypothesized sensorimotorcortical integrators. The 3×3 diagonal matrices $\mathbf{F}_2$ and $\mathbf{MC}$ affect the relative balance of cortical and cerebellar circuitries. Proprioceptive feedback processing accesses the cerebellar system directly through $\mathbf{F}_2$. Descending signals from parietal or motor cortices that bypass the cbCtx are scaled by $\mathbf{MC}$.

A very similar scheme that includes activity related to a reverberating circuit between $\mathbf{u}_{\text{cb}}$ and $\mathbf{x}_{\text{cb}}$ involving precerebellar brainstem nuclei (Allen and Tsukahara 1974) is taken to implement integration (Massaquoi 1999; Massaquoi and Topka 2002). A mechanism similar to that producing recurrent integration for band-limited differentiation (Figure 2c) is assumed to also provide descending integration. This integral signal is scaled by the 3×3 diagonal matrix I_2 and projected to cerebral cortex in a recurrent feedback manner. The circuit has closed-loop transfer matrix $\text{s}\mathbf{I}(\text{s}\mathbf{I} + \mathbf{I}_2)^{-1}$ (where $\mathbf{I}$ is an identity matrix) and provides significant phase lead that is responsible for delay compensation.

In particular, examining for simplicity a single joint representation in terms of scalars $g_{\text{k}}, i_1, i_2, f_2, i_{\text{a}}$, and mc in Fig. 3, the transfer function from x_{c} to u_{cb} is given by $(sg_{\text{k}} + i_1)/(s + i_2)$, and the overall transfer function from Θ to u_{mc} is $-(sg_{\text{k}}f_2 + i_1 f_2 + g_{\text{k}}i_{\text{a}} + i_1 i_{\text{a}}/s)/(s + i_2) - i_{\text{a}}\text{mc}/s$, and therefore for $|s| << i_2$, this becomes $-(i_1 f_2/i_2 + g_{\text{k}}i_{\text{a}}/i_2) - (i_1 i_{\text{a}}/i_2 + i_{\text{a}}\text{mc})/s - s(g_{\text{k}}f_2/i_2)$. Thus, for lower frequencies, proprioceptive control is approximately PID. However, it should be noted that inclusion of excitation–activation muscular dynamics [Equation 9] renders the control between $\mathbf{\Theta}$ and $\boldsymbol{\tau}_{\text{M}}$ to be slightly more complex than PID even before force feedback is included.

The FRIPID model adds a torque feedback loop that represents force-related information from the pressure distribution on the feet or muscle tension sensed by Golgi tendon organs (Peterka 2003). For the moment, it is assumed that this signal traverses the cerebral cortex where force information is felt to arrive at the cerebral cortex via the VPL thalamic nucleus (Brodal 1981). By symmetry with the processing of proprioceptive information in the basic RIPID model and consistent with the predominantly low-frequency effect of force feedback as explored by Peterka (2003), force feedback is processed by a (thalamo-) cortical integrator associated with 3×3 scaling matrix I_{τ}.

Closed-loop transmission delays through spinal and peripheral nerves ($\mathbf{T}_{\text{spr}}$) are conservatively taken to be 60, 70, and 80 ms for long-loop responses to and from the hip, knee, and ankle, respectively, based on 2 m height, 50 m/s neural conduction velocity, and five synaptic delays of less than 1 ms.

It was also found empirically that the use of feedforward muscular coactivation in concert with long-loop control improved the fit to some human datasets. It was assumed that for healthy subjects, the magnitude of this component should be comparatively small. However, it was suspected a priori based on clinical observations (Massaquoi and Hallett 1997) that coactivation might be increased to compensate for degraded cerebellar processing of long-loop responses. To accommodate this, the FRIPID model was augmented by a hypothetical system that triggered a prespecified level ($\mathbf{CA}$) and duration of muscular coactivation when a sufficiently large ankle velocity signal was detected at the cortex.

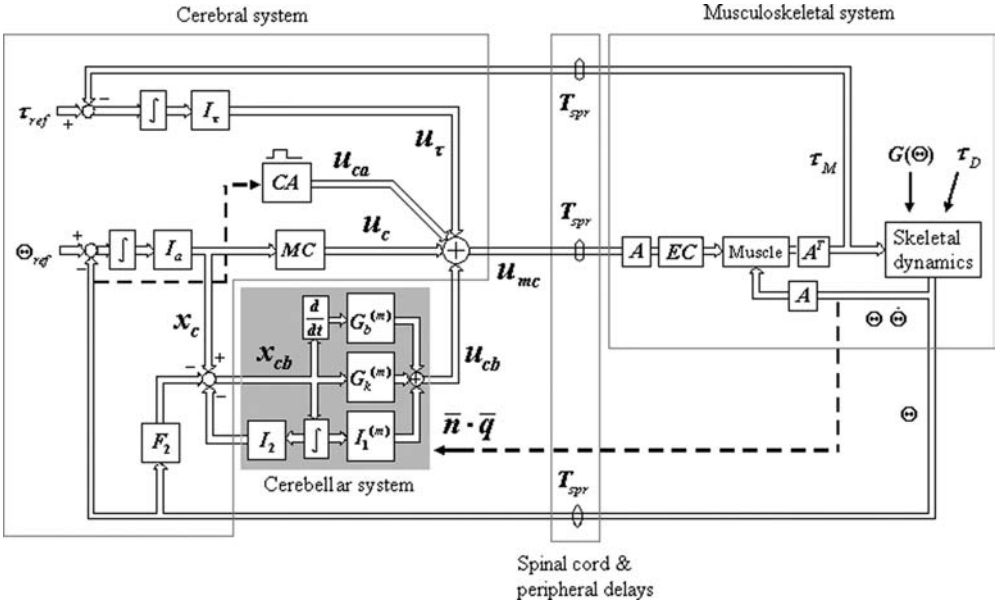

Fig. 3. Force feedback RIPID cerebrocerebellar balance control model (see text for explanation of features)

2.2.3 Cerebellar control gainscheduling. Preliminary simulations demonstrated that, while a basic balance control RIPID model can recover upright posture following gentle platform disturbances, it was inadequate for more violent disturbances. Many investigators (Brindley 1969; Ito 1972; Thach et al. 1992a; Wolpert et al. 1998) have considered the possibility that the cerebellar function varies with physiological context. As the cerebellum receives rich input from many parts of the body, and Purkinje cell activity has been related to joint kinematic activity (Johnson and Ebner 2000), it is highly conceivable that different corticonuclear microcomplexes become active in different kinematic states. A straightforward application of this idea to the FRIPID model is therefore the proposition that the cerebellar system gains $\mathbf{G}_{\mathrm{b}}^{(m)}$, $\mathbf{G}_{\mathrm{k}}^{(m)}$, and $\mathbf{I}_{1}^{(m)}$ may be scheduled according to sensed kinematic state.

Figure 4 shows a simple proposal for a gainset selection mechanism in which a "beam" of activity on *suppressor* parallel fibers ($\mathrm{PF_{sup}}$) inhibits (via basket cells, not depicted explicitly (Eccles et al. 1967; Ito 1984)) Purkinje cells some distance away ("off beam"). This diminishes the net inhibition in those modules, allowing them to process the input x_{cb} that arrives on *signal* parallel fibers ($\mathrm{PF_{sig}}$). Conversely, the beam activates local Purkinje cells, thereby suppressing the activity of "on beam" modules. The principal characteristic required of $\mathrm{PF_{sup}}$ fibers in this scheme is that, unlike $\mathrm{PF_{sig}}$ fibers, they should contact Purkinje cells relatively more strongly than the corresponding deep nuclear cells – if they contact the same DCN cells at all. This appears to be generally consistent with the studies of Eccles et al. (Eccles et al. 1974a,b; Ito 1984). A prime candidate source for suppressor PF is the dorsal spinocerebellar tract (DSCT) elements, which are known to convey mixtures of proprioceptive and other information from multiple muscles within a limb (Oscarsson 1965; Bloedel and Courville 1981; Osborn and Poppele 1992) while typically maintaining a steady level of background firing in the absence of afferent input (Mann 1973). We may formalize these observations by proposing that the DSCT fibers transmit $[\bar{\mathbf{n}}_{\mathrm{i}} \cdot \bar{\mathbf{q}}]_+$, where $\bar{\mathbf{q}} = [\hat{\theta}_1 \quad \hat{\theta}_3 \quad \hat{\dot{\theta}}_1 \quad 1]^{\mathrm{T}}$ and $\bar{\mathbf{n}}_i = [\mathbf{n}_i - n_{0i}]^{\mathrm{T}}$ for many different values of directional unit vector $\mathbf{n}_i$ and offset n_{0i}. It would be expected that, in vivo, $\bar{\mathbf{q}}$ would be the average signal of a large number of primary afferents (Mann 1973), thereby reducing the noise transmitted to the cerebellum. Thus, certain suppressor fibers become relatively more active when the sensed kinematic state is located in a region of the state space bounded by the plane perpendicular to $\mathbf{n}_i$ at distance n_{0i} from the origin. Depending upon the signs of $\mathbf{n}_i$ and n_{0i}, the region may or may not include the origin (Fig. 5). The net gainscheduling action can therefore be written as:

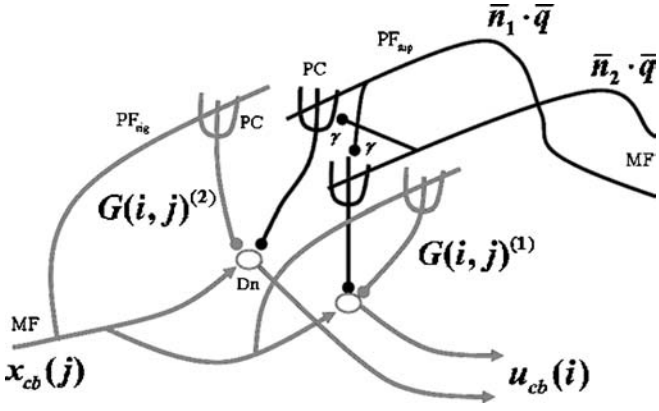

Fig. 4. A model of proposed gainscheduling circuitry in CbCtx; Mossy fibers (MF), parallel fibers (PF), Purkinje cells (PC), and cerebellar deep nuclear cell (Dn)

$$G(i,j) = G(i,j)^{(1)}[1-[1-\gamma[\bar{\mathbf{n}}_1 \cdot \bar{\mathbf{q}}]_+]_+]_+ + G(i,j)^{(2)}[1-[1-\gamma[\bar{\mathbf{n}}_2 \cdot \bar{\mathbf{q}}]_+]_+]_+ , \qquad (11)$$

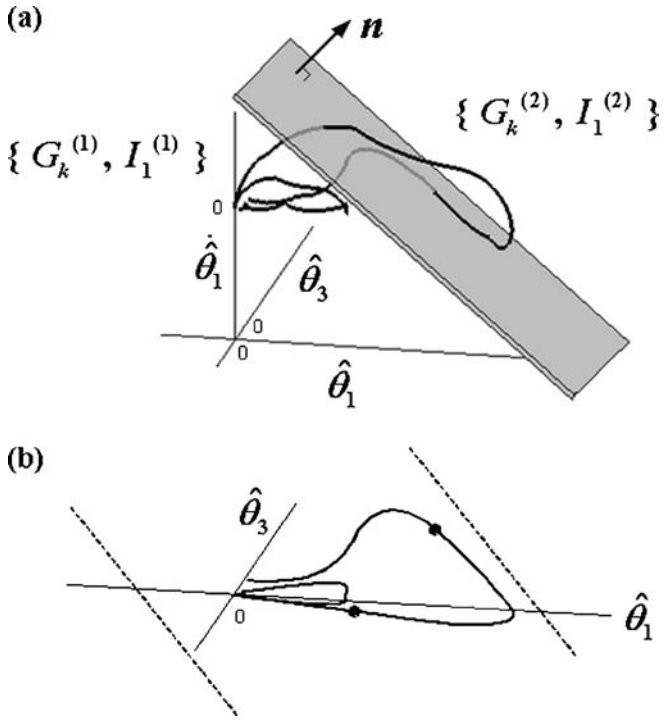

Fig. 5. **a** Two sensed (delayed) recovery trajectories and one (for clarity) of two closely spaced parallel switching planes separating gainset regions in $\hat{\theta}_1 \times \hat{\theta}_3 \times \dot{\hat{\theta}}_1$ space. **b** Projection of sensed trajectory onto $\hat{\theta}_1 \times \hat{\theta}_3$ space with two large dots corresponding to points of their intersection with switching plane. *Dashed lines* show approximate limits of feasible balance region as in Fig. 6

where γ represents the strength of lateral inhibition provided by basket cells. This parameter regulates the steepness of the transition zone between scheduling regions.

2.3 Simulations of physiological and pathological balance control

Several experimental methods have been employed to study human balance control (Horak and Nashner 1986; Nashner and McCollum 1985), including platform translations. Humans have been noted to exhibit characteristically different balancing kinematics that *emphasize* either ankle or hip motion depending upon the magnitude and speed of the platform disturbance. Backward platform movement and kinematic data in Henry et al. (1998), Runge et al. (1999), and Park et al. (2004) covered a fairly wide range of disturbance velocities, but they were not identical. Also, platform kinematics were not reported in detail. These studies were used to establish a useful set of nominal model gains with respect to which other changes were made as described.

For simulations, platform movements were 2.97-, 4.50-, 5.94-, 6.75-, and 9.00-cm displacements lasting 300 ms and were sigmoidal in time. An important check on the presumed cerebellar locus of the control system is whether simulated lesions yield balance control deficits that correspond to clinical findings. In particular, diffuse cerebellar injury, especially of the anterior lobe that results in general loss of cerebellar tissue (atrophy), would be expected to reduce the strength of the cerebellar gains. It is also conceivable that this deficit might engender increased active muscular stiffness from the cerebral cortex and/or elsewhere to help compensate for the loss of long-loop control.

No attempt was made to obtain precisely optimal fits according to any abstract mathematical cost function. Rather, reproduction of human behavior was sought that yielded approximate that were visually satisfactory. The tuning procedure involved first obtaining a stabilizing linear quadratic regulator (Franklin et al. 1994) that approximated human behavior for small disturbances. Then, the behavior was tuned manually to fit human data with force feedback and muscular coactivation.

3 Results

Successful balancing reactions to the full range of tested disturbances were achieved by the FRIPID model using just two, slightly overlapping, gainscheduling regions in $\hat{\theta}_1 \times \hat{\theta}_3 \times \dot{\hat{\theta}}_1$ space. In principle, there is no reason to expect that the cerebellum does not have access to the equivalent of full state information from all joints. However, we sought the smallest number of kinematic variables that could enable the model's switching mechanism to account for the data. The components $\hat{\theta}_1$ and $\hat{\theta}_3$ provide significant information about the body's center of mass when there is little knee motion, and $\dot{\hat{\theta}}_1$ provides rapid information about platform velocity. Figure 5 depicts the projection of a low-velocity and high-velocity recovery trajectory into this subspace and the scheduling zones determined by two closely spaced planes. The planes are defined by the equations:

$$\bar{\mathbf{n}}_i \cdot \bar{\mathbf{q}} = 0, i = 1, 2. \tag{12}$$

For the simulation, $\bar{\mathbf{n}}_1 = [-0.992 \;\; 0.111 - 0.061 \;\; 0.773]^{\mathrm{T}}$, $\bar{\mathbf{n}}_2 = [0.992 - 0.111 \;\; 0.061 - 0.605]^{\mathrm{T}}$.

The quantity $[\bar{\mathbf{n}}_1 \cdot \bar{\mathbf{q}}]_+$ is positive for sensed state space locations on the origin side of the outer plane. $[\bar{\mathbf{n}}_2 \cdot \bar{\mathbf{q}}]_+$ is positive at locations beyond the inner plane. The inner part of the space was considered the *base region*, and its associated gain matrices $\mathbf{G}_{\mathrm{k}}^{(1)}, \mathbf{I}_1^{(1)}$ yielded ankle strategy. The outer zone, designated the *catching region*, was associated with $\mathbf{G}_{\mathrm{k}}^{(2)}, \mathbf{I}_1^{(2)}$ and generated mixed ankle-hip strategy.

A number of human studies have shown the same basic patterns of body movement in relation to platform translation (Henry et al. 1998; Runge et al. 1999; Park et al. 2004; Allum and Honegger 1992; Horak and Nashner 1986; Nashner and McCollum 1985). Figure 6 shows the model tuned to most closely approximate the data of Henry et al. (1998). Attention is paid here to the relative amplitudes and timings of the joint excursions and smoothness of settling. It is noteworthy that, although the joint angle vs. time plot of the data of Henry et al. did not show initial hip undershoot, the ankle-hip body configuration trajectory plot did (Henry et al. 1998, Fig. 2). We consider the

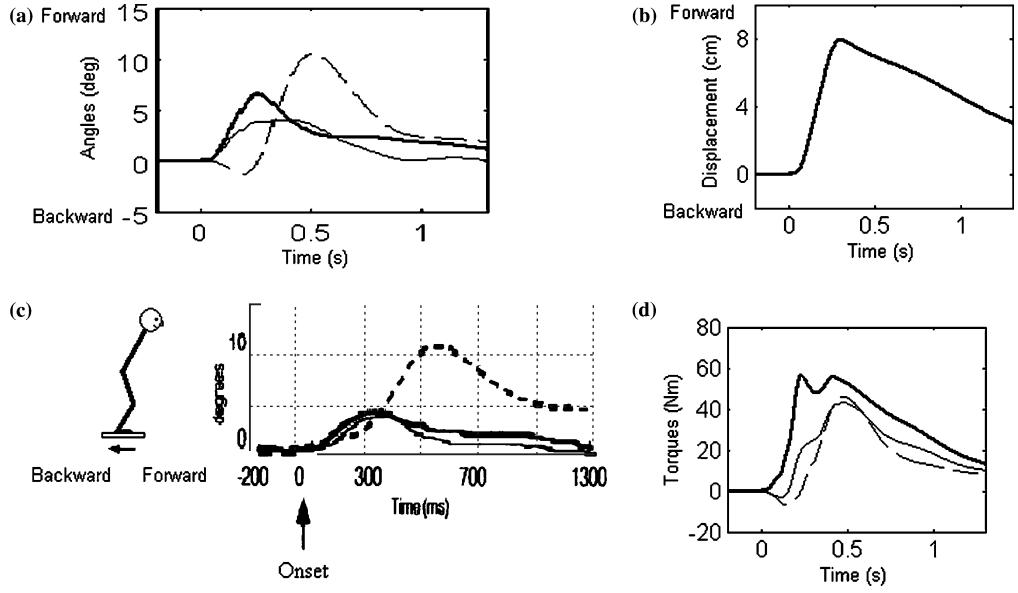

Fig. 6a–d. *Left* (**a**) Simulated and (**c**) actual (Henry et al. 1998; with permission from IEEE Transactions on Rehabilitation Engineering for Reproduction) kinematics showing ankle (*thick solid line*), knee (*thin solid line*), and hip (*dashed line*) motion in response to backward platform movement. *Right*: (**b**) Simulated c.o.m. trajectory and (**d**) simulated torque profiles

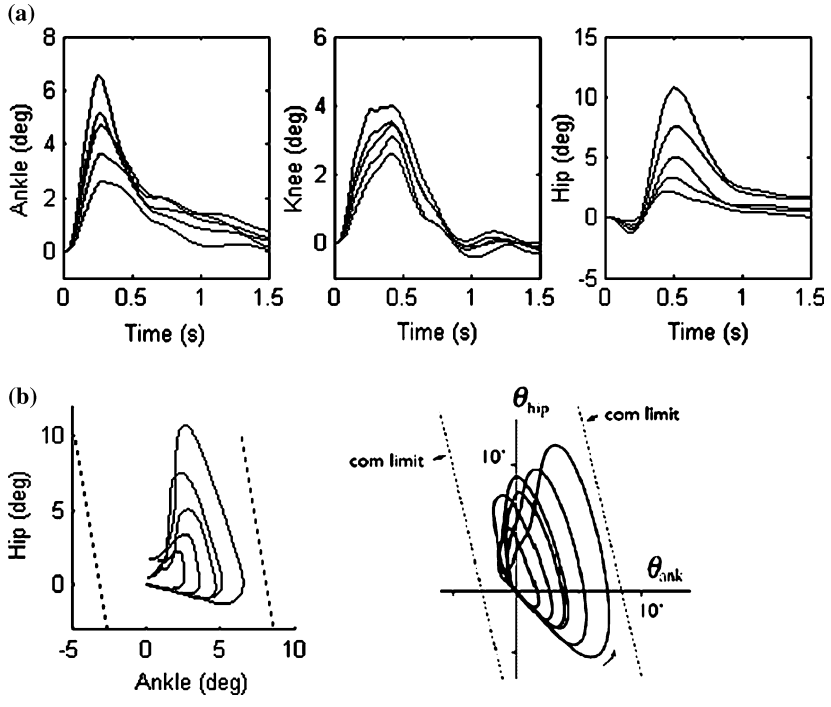

Fig. 7. a Simulated joint trajectories for a family of different sized disturbances (details in Sect. 2.3). **b** *Left*: Simulated ankle vs. hip configuration plots. *Right*: Configuration plot adapted from Park et al. (2004); with permission from Experimental Brain Research for Reproduction. *Dotted lines* indicate boundaries in ankle-hip joint space where c.o.m. remains within feasible region for balance

possibility that in this study the feature was variable and was averaged out in the time domain plot. Other studies have typically shown initial hip motion undershoot (Fig. 5 in Park et al. 2004; Fig. 3 in Runge et al. 1999), as does the simulation. The simulated vertical projection of the center of mass onto the ground remains within the base of support assuming a length from the ankle to the first metatarsophalangeal joint of at least 8 cm, which is a conservative estimate, and the peak ankle torque remains below 60 Nm, a value which Park et al. (2004) found to be consistent with the heels remaining flat on the platform. From this point on, we will refer to the parameter settings used in the top left of Fig. 6 as the base FRIPID scheduled control model.

The responses of the scheduled FRIPID model to displacements of different velocities are shown in Fig. 7. If the generally small variation in knee angle motion is neglected, the body configurations that are consistent with balance can be determined to lie approximately between the diagonal dashed lines shown. The "strategy" being implemented can be characterized by assessing the determinants of center of mass (c.o.m.) control. Slow disturbances result in comparable peak excursions at the ankle and hip. In this case, because the body center of mass is much farther from the ankle than the hip, ankle motion has the dominant control over c.o.m. positioning and, therefore, over balance. This type of motion is considered "ankle strategy" (Nashner and McCollum 1985). On the

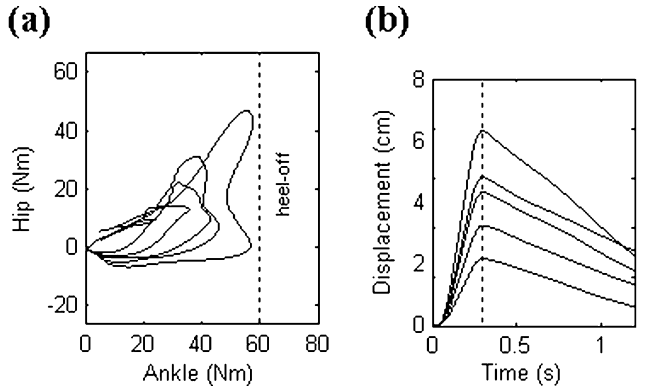

Fig. 8. **a** Simulated hip vs. ankle joint torque trajectories. The *dotted line* indicates the maximum allowable ankle torque for which feet remain flat on the ground [as indicated in Park et al. (2004)]. **b** Trajectories of c.o.m. forward displacement corresponding to different platform velocities. The *dotted line* indicates the time at which platform movement ends

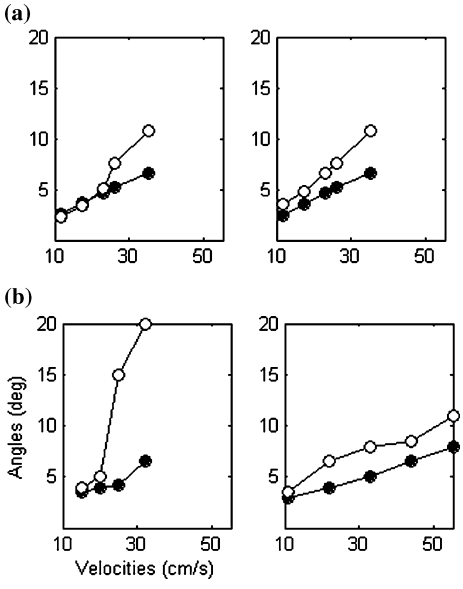

Fig. 9a, b. Peak values of ankle (*solid*) and hip (*open*) angles vs. platform velocity. **a** Simulations with different cocontractions. **b** Actual data from Runge et al. (1999) (*left*) and Park et al. (2004) (*right*)

other hand, rapid disturbances yield progressively greater hip motion until both joints contribute more equally to balance, especially later within the recovery motion. This pattern may be termed "mixed ankle-hip strategy". It enables the body to remain within the feasible balance configuration region by limiting ankle movement and restricting ankle torque to levels consistent with maintaining heel contact with the platform (Fig. 8a). The flexion at the hip and extension at the ankle that promote c.o.m. recovery are aided by the abrupt deceleration of the platform at all translational velocities, as was described by Runge et al. (1999). The same pattern of platform promotion of c.o.m. recovery was noted in the simulations (Fig. 8b). The base FRIPID scheduled control model settings produce a distinct transition between strategies at a platform velocity of about 25 cm/s, qualitatively similar to the data of Runge et al. (1999) (Fig. 9).

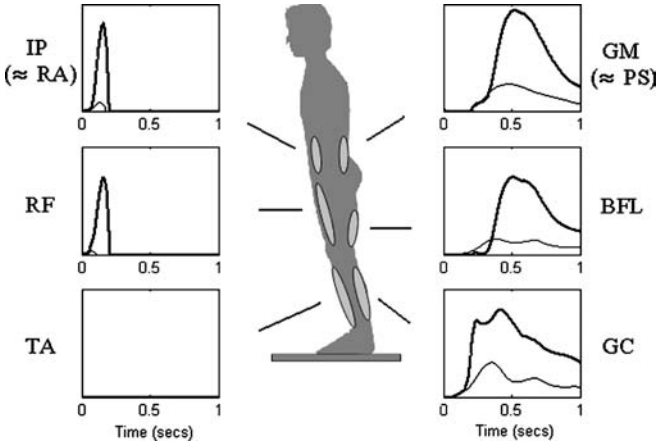

Fig. 10. Simulated EMGs in low-velocity (*thin lines*) and high-velocity (*thick lines*) platform disturbances. *PS* paraspinals, *RA* rectus abdominis

Figure 10 shows the distribution of simulated electromyogram (EMG) activity: $[l(u_k) - l_k]_+$, for six muscles, k. Horak and Nashner (1986) recorded hip joint EMG from rectus abdominis (RA) rather than iliopsoas, and from paraspinals (PS) rather than gluteus maximus. The RA and PS have mechanical functions very similar to the PS and GM and were found to show similar EMG patterns. The two principal EMG features are that for low disturbance velocities there is extremely little activation of ventral musculature while the dorsal muscles are activated in ascending sequence, despite the shorter long-loop reflex times of the knee and hip musculature. This is a recognized pattern in ankle strategy motions (Horak and Nashner 1986). Second, at higher velocities there is early activation of ventral muscles at the knee and hip and late activation of the dorsal muscles at these joints. This is the characteristic muscle activation pattern associated with mixed ankle-hip strategy (Horak and Nashner 1986). Tibialis anterior (TA) activity varies between studies from zero for all velocities as predicted here to zero only for low velocities. This may be related to varying levels of coactivation at the ankle.

The contributions of different proposed CNS signal components to the three joints are shown in Fig. 11 for the base model. For all joints, the cerebellum contributes the largest signals. The signal spike is related to the time of gainset transition. It generally does not manifest itself in the EMG due to low-pass EC filtering. Force feedback contributes to ankle and hip control gradually. Even at high disturbance velocities as shown here, ankle activation is strongest (note the different scales). This is presumably related both to the larger torque requirement and to the relatively less inherent stiffness of ankle muscles in comparison to larger muscles above. Knee activation is always quite modest. Muscular cocontraction contributes very slightly to the ankle, but significantly to the knee, to minimize buckling. The time course of u_{ca} was determined empirically to improve fit with data.

The FRIPID model qualitatively reproduces the postural disturbance responses of persons with cerebellar disease, especially of the anterior lobe as in nutritional deficiency-related cerebellar degeneration (Massaquoi

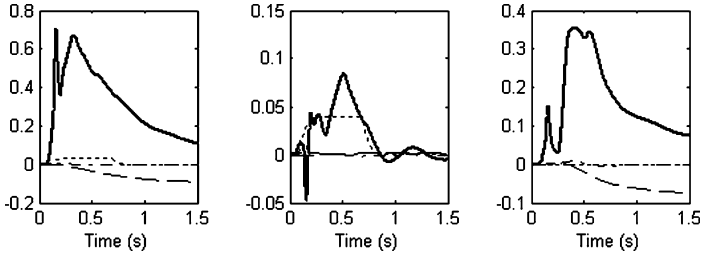

Fig. 11. Simulated cerebrocerebellar signals descending to ankle, knee, and hip, respectively, from *left* to *right*: *thick line* u_{cb}, *dotted line* u_{ca}, *dashed line* u_{τ}, *dash-dotted line* u_c

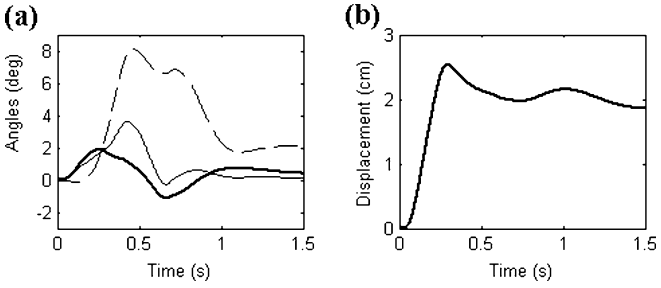

Fig. 12a, b. Predicted response of person with cerebellar disease to a low-velocity (11.55 cm/s) backward platform disturbance. **a** Simulated joint trajectories: ankle (*thick solid line*), knee (*thin solid line*), and hip (*dashed line*). **b** Simulated c.o.m. trajectory

and Topka 2002) in Fig. 12. To simulate cerebellar disease, the magnitudes of cerebellar control gains ($\mathbf{G}_k^{(m)}, \mathbf{I}_1^{(m)}$) were reduced by 40%. This would correspond to loss of deep cerebellar nuclear cells, mossy or PF with or without Purkinje cell loss. On the other hand, muscular coactivation was increased to simulate the apparent typical compensation strategy employed by patients. A relatively mild ramp platform displacement of 3 cm over about 300 ms was applied to qualitatively reproduce experimental observations of Horak and Diener (1994). Consistent with clinical observations, patients develop significantly larger amplitude ankle and hip motions but only relatively minor disturbance in c.o.m. location. Thus, patients tend to oscillate, but not fall, unless they trip. In simulations, it was also noted that body oscillation may become more sustained, yielding a typically 2- to 3-Hz postural tremor termed titubation (Massaquoi and Topka 2002). It is apparently engendered by the muscular coactivation and/or by reduction in recurrent integrator function associated with reduced $\mathbf{I}_2$ (Massaquoi and Hallett 1998).

4 Sensitivity analysis

Aside from the changes in parameters that correspond to damage to the cerebellum itself, the sensitivity of the model to other components was explored as shown in Fig. 13. Principal observations are: First, as expected, model function is most sensitive to the integrity of $\mathbf{I}_2$ the recurrent integrator path gain and $\mathbf{F}_2$ the gain of direct long-loop feedback to cerebellum. The former may be reduced by interruption of cerebellar outflow destined for the cortex as often occurs in multiple sclerosis and gives rise to a violent, destabilizing tremor that may affect arms or body. Attenuation of the latter signal as occurs with deafferentation by peripheral sensory nerve or spinal disease may be compensated for by visual input to some extent. Eye closure results clinically in the catastrophic fall depicted here. Moderate changes in the cerebellar gainsets or switching in general provide appreciable but generally modest changes in balancing motion trajectory. This is appropriate for an adaptive control mechanism. The relevance of gainset switching is shown by raising the switching plane to greater than 200% of its setting in the base model. In this case, only ankle strategy occurs. Although the c.o.m. excursion increases only slightly, the peak ankle torque rises to 70 Nm, thereby exceeding the criterion for maintaining heel contact on the platform. The marked robustness of the control system to increases in neural signal transmission delays is demonstrated by the less than 2% increase in c.o.m. excursion engendered by a 40% increase in loop transmission time. Force feedback is necessary to prevent violent recoil of the ankle that could otherwise be destabilizing as described earlier. Finally, muscular coactivation is not necessary for balance recovery. However, it does enhance the speed of c.o.m. return to zero.

5 Discussion

The present study demonstrates that the combination of stabilized, scheduled long-loop proprioceptive and force feedback could provide flexible and powerful control to facilitate postural defense despite the presence of significant signal transmission delays and phase lags. Negative force feedback attenuates the otherwise large and potentially injurious or destabilizing force transients that could be engendered more often by PID control alone. The findings also suggest that the body's control could be substantially linear within regions of the kinematic state space with switching driven by a small number of sensed variables. The control segmentation need not be fine-grained, and there is apparently no requirement for precise prediction of body state that would necessitate an internal forward dynamics model. Finally, the ability to reproduce at least qualitatively the balance dysfunction in cerebellar disease supports the model's attribution of long-loop scaling and stabilization to cerebellar circuitry.

It has already been shown (Kuo 1995) that for disturbances of the magnitude that occur within these experiments, human body dynamics can be effectively linearized. Therefore, in the context of effective full body state estimation/prediction by a linear internal dynamics model, it is possible to reasonably describe human responses to platform translation in terms of optimal

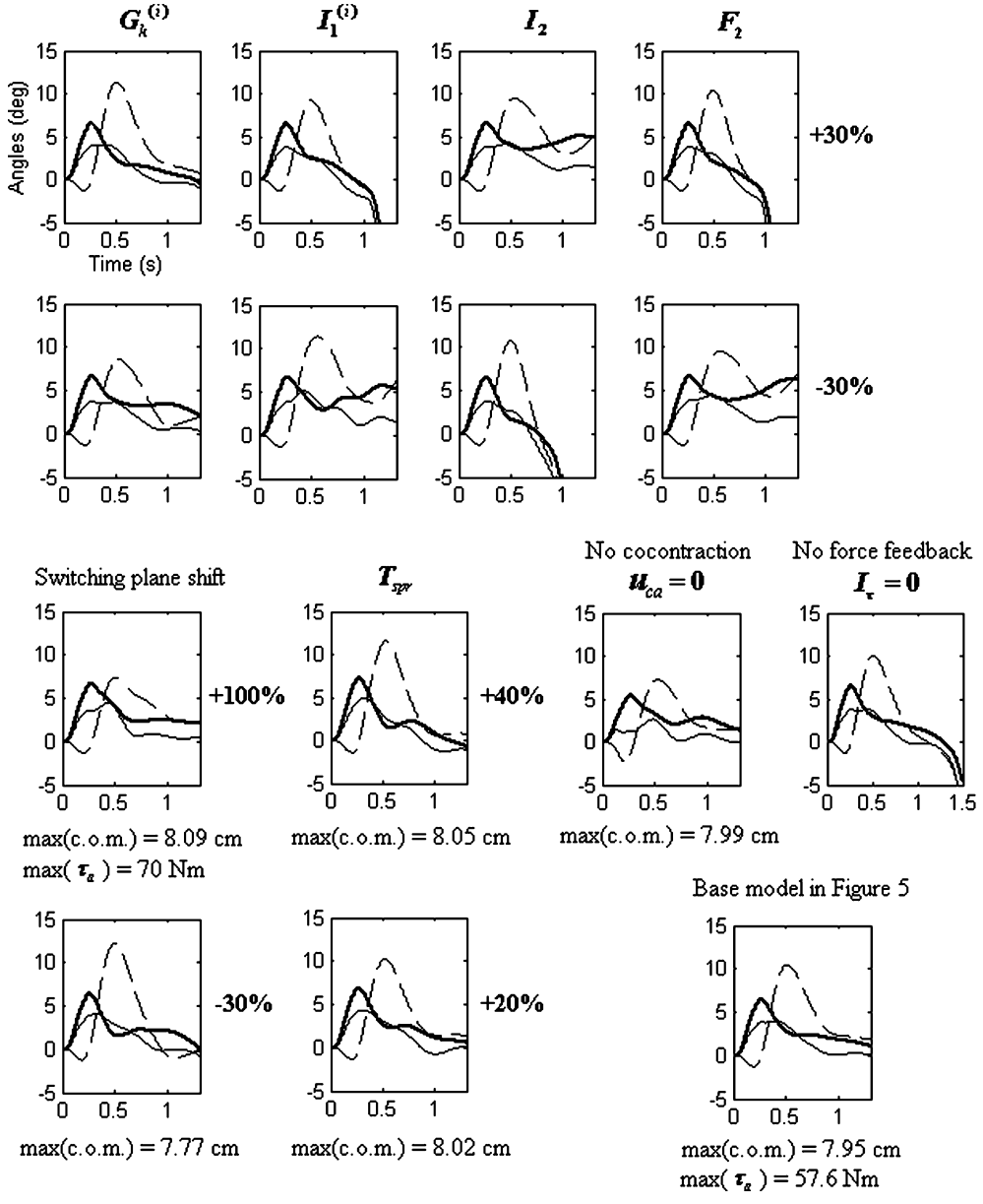

Fig. 13. Sensitivity to several parameters: ankle (*thick solid line*), knee (*thin solid line*), and hip (*dashed line*) motions. *max* (*c.o.m.*): the maximum value of forward c.o.m. displacement, *max* (τ_a): the maximum value of ankle torque trajectory

linear (linear quadratic Gaussian) control (Kuo 1995). In this and other models (Hemami and Katbab 1982; Miall et al. 1993), the control portion as opposed to estimation component is designed as if there were no delays. Studies (Miall et al. 1993) have argued that the experimental disruption of visuomotor tracking produced by delays is consistent with the presence of an internal dynamics model used for prediction of target motion and internal feedback signals. And, more generally, the potential advantages of physiological model-based state estimation have been well summarized (Wolpert et al. 1995). However, it has not been established that such internal models exist, and even if some do, low-level subconscious proprioception-dependent all of postural control does not necessarily depend upon all of the same mechanism as does visuomotor tracking.

The distinction between high-level tracking and low-level body stabilization is potentially important for any animal in an open environment where body motion in the context of novel loads may not be well predicted by existing internal dynamics models. If control system stability depended sensitively on state estimation/prediction, then the estimator would have to be accurately updated during the motion itself. This would be especially challenging in high-speed multijoint, environmentally interactive behaviors such as predation. It is not clear where or how such learning would likely occur in the CNS. Effective adaptation in cerebellum, basal ganglia, and motor cortex seems to require at least several repetitions of movement even under constantly maintained novel conditions (Martin et al. 1996; Tremblay et al. 1998; Li et al. 2001). Continuous reorganization of cerebral sensory cortical activity does not seem to be a likely candidate for improving low-level control on the scale of fractions of a second. And spinal circuitry does not appear to have the requisite complexity for such flexible general-purpose internal

modeling. On the other hand, if the control scheme does not require accurate estimation/prediction of body state or environmental forces, then internal forward dynamics and/or delay models may not be needed. In this case, the computational circuitry may be simpler, the stability and performance more robust, and the adaptation allowed to proceed at a more moderate rate.

Proportional integral derivative (PID)-type control formulas have been used to describe frequency domain characteristics of human body sway involving primarily ankle motion (Johansson et al. 1988; Peterka 2001). However, balance maintenance in reaction to rapid external disturbances necessitates multijoint, e.g., mixed hip and ankle, responses. And rapid disturbances may excite high-frequency dynamics that give rise to undesirable oscillations or destabilize a nonlinear system with delays or other phase lags. Therefore, it must be explicitly verified that PID control can be extended to explain the kinematics of both gentle and more violent disturbance recoveries. Moreover, it is desirable to determine how such control may be implemented physiologically.

The RIPID models (Massaquoi 1999) were developed in the context of wave-variable teleoperation ideas (Niemeyer 1996) as an effort to account for the apparent robustness of the animal motor control system to time delays and phase lags. Wave variables are linear combinations of velocitylike and force signals that can be exchanged between a master site and a remote slave site in a manner that can ensure stable feedback control over any distance and with any object so long as the remote environment and load are passive. Wave-variable-based models of animal motor control have been investigated and proposed (Massaquoi 1999) with some ability to account for both input-output arm movement control and nonvertical postural stability, and possibly several internal signals observed experimentally. The RIPID models use the core simplicity of the wave-variable approach without fulfilling all of the latter's formal requirements. As such, RIPID stability tends to be quite robust under the typical operating conditions of human arms, although it is not guaranteed.

Managing the dynamics of upright posture presents a particular challenge for the purely proprioception-based RIPID models. First, the plant is inherently unstable due to an external force that varies nonlinearly with respect to body configuration, potentially accentuating the destabilizing effects of control system delays. Second, in the presence of external forces, applied muscular torque cannot be deduced from kinematic state alone without an internal model of the kinematics–force relationship if such could be known. Third, the goal of upright balance is not necessarily the immediate return to vertical. Rather, it is, first, roughly to prevent excursion of the vertical projection of the center of mass beyond the base of support, and secondarily to return to vertical at a comfortable rate. In certain high performance situations, the latter phase may not even be required. Thus, early simulations indicated that the scheduled, purely proprioception-based RIPID model could not account well for natural postural recovery kinematics without resorting to multiple, precisely timed switches in controller gains. While not physiologically inconceivable, this lack of robustness was unattractive.

The inclusion of negative force feedback significantly improved the realism of the RIPID model responses. To investigate the most challenging possibility with regard to delay-engendered instabilities, a transcortical path was simulated. However, the long-loop processing of force information is not well understood. It is conceivable that shorter paths involving only the cerebellum might be most important. In any case, it was still found to be necessary to posit that a different gainset became active as disturbances became more violent. Relatively simple interpolation between the gainsets on the basis of sensed kinematic state was found to be sufficient even with sensing time lags. The proposed gainset selection mechanism based on sensed state represented by augmented vectors $\bar{n}_i$ is simple and flexible. Though clearly speculative, it appears to be consistent with an implementation by spinocerebellar pathways that apparently carry a mixture of signals from the periphery (Osborn and Poppele 1992) and with previous proposals for operation of cerebellar corticonuclear circuitry (Eccles et al. 1967; Ito 1997). It has a flavor similar to the expansive recoding of kinematic state used by Kettner et al. (1997). However, the function of this input is purely one of gainset selection, not in direct generation of a control output. With force feedback incorporated, only two cerebellar gainsets were needed to achieve realistic kinematics with appropriate limitation of c.o.m. excursion and peak ankle torque. This represents a significant improvement in efficiency and robustness of stability with respect to prior efforts (Jo 2002). Importantly, a 40% increase in loop signal transmission time accentuated hip and ankle motions but resulted in only a trivial decrease in c.o.m. control. Still, the mechanism by which appropriate gainsets would be learned within the cerebellum is not clear. This remains an important issue for physiological credibility and is therefore an important target for future investigations.

That the FRIPID model yielded simulated EMG patterns with several semiquantitatively realistic features is not completely trivial because of the redundancy of musculature around joints and the possibility of muscular coactivation. Thus, EMG patterns are not fully determined by the kinematic behavior of the body model. On the other hand, the exploration of muscle activation patterns was very limited in this study. More sophisticated muscle models that include continuously varying activation-dependent stiffness and segmental stretch responses would be essential for future efforts in this direction.

The finding that central features of the abnormal balance displayed by persons with cerebellar disease could be approximated at least qualitatively by reducing the gains of the cerebellar component of the model mirrors a similar finding in the modeling of arm control (Massaquoi 1999). The further improvement in realism by the addition of muscular coactivation appears reasonable, though it remains somewhat speculative. Enhancement of extracerebellar long-loop responses might have a similar effect. Perhaps both changes occur. In any case, simulating the

effects of cerebellar system lesions further supports the neuroanatomical specificity and architecture of the model. In this regard, we found it very interesting that $\mathbf{G}_{\mathrm{b}}^{(m)}$ gainsets were not needed for the balance task studied. In retrospect, this was likely attributable to the fact that the desired recovery motions of the body segments did not contain high frequencies. In the RIPID model, the $\mathbf{G}_{\mathrm{b}}^{(m)}$ are used to scale differentiated signals attributed to lateral cerebellum whose output is through the Dn (Massaquoi 1999). While it has been noted that there is apparently a complete somatotopic body representation of within the dentate (Thach et al. 1992b), the dentate is generally seen to be less active with truncal and leg movements than with arm and hand movements. This is especially true in comparison with the activity of the interpositus and the fastigial nuclei, which we associate more strongly with $\mathbf{G}_{\mathrm{k}}^{(m)}$ and $\mathbf{I}_{1}^{(m)}$ and which are known to be strongly involved in proximal arm and truncal control. This suggests that the apparent difference in the distal-to-proximal preferences of dentate and interpositus control may be related to differences in the frequency content of typical body segment movements.

While the findings of this study do not preclude the presence of more complex processing in the cerebellum, we find the potential simplicity and applicability of RIPID-type models to different control problems appealing. Still, model behavior must be examined with respect to a much larger set of experiments to confirm this impression. An anatomically more detailed version of the RIPID model has already been used to account for a number of internal signals within the motor system during arm movement (unpublished). Ultimately, it would be important to test the FRIPID model against recordings from primate cerebellar neurons during upright stance, but we are not aware that such datasets exist.

Appendices

A The dynamic equations of motion

A three-link inverted-pendulum model represents the model of human body with three segments, e.g., lower leg, upper leg, and trunk. The segments are connected by frictionless hinge joints, and the feet remain flat on the ground.

The m_i is the mass of a segment i, l_i is the length of a segment i, and h_i is the moment of inertia of a segment i at center. Segment 1 is the lower leg, 2 is the upper leg, and 3 is the trunk. Body model parameter values are: $m_1 = 4$ kg, $m_2 = 7$ kg, and $m_3 = 49$ kg; $l_1 = 0.4$ m, $l_2 = 0.5$ m, and $l_3 = 0.8$ m; $h_1 = 0.12$ kgm^2, $h_2 = 0.14$ kgm^2, and $h_3 = 2.3$ kgm^2; and $g = 9.81$ m/s^2 (adapted from Van der Kooij et al. 1999).

$$\mathbf{H}(\mathbf{\Theta})\ddot{\mathbf{\Theta}} + \mathbf{C}(\mathbf{\Theta}, \dot{\mathbf{\Theta}}) = \boldsymbol{\tau}_{\mathrm{M}}(\mathbf{\Theta}, \dot{\mathbf{\Theta}}, \mathbf{u}_{\theta}) + \boldsymbol{\tau}_{\mathrm{D}}(\ddot{\mathrm{D}}, \mathbf{\Theta}) + \mathbf{G}(\mathbf{\Theta})$$

$$\mathbf{M}(\mathbf{\Theta}) = \begin{bmatrix} M(1,1) & M(1,2) & M(1,3) \\ M(2,1) & M(2,2) & M(2,3) \\ M(3,1) & M(3,2) & M(3,3) \end{bmatrix},$$

$$\mathbf{C}(\mathbf{\Theta}, \dot{\mathbf{\Theta}}) = \begin{bmatrix} C(1) \\ C(2) \\ C(3) \end{bmatrix},$$

$$\mathbf{G}(\mathbf{\Theta}) = \begin{bmatrix} G(1) \\ G(2) \\ G(3) \end{bmatrix}, \quad \boldsymbol{\tau}_{\mathrm{D}}(\ddot{\mathrm{D}}, \mathbf{\Theta}) = \begin{bmatrix} W(1) \\ W(2) \\ W(3) \end{bmatrix}.$$

$$\begin{aligned}
M(1,1) &= h_1 + h_2 + h_3 + m_1 r_1^2 + m_2(l_1^2 + r_2^2) \\
&\quad + m_3(l_1^2 + l_2^2 + r_3^2) + 2(m_2 l_1 r_2 + m_3 l_1 l_2) \\
&\quad + 2m_3 l_2 r_3 \cos\theta_3 + 2m_3 l_1 r_3 \cos(\theta_2 + \theta_3) \\
M(1,2) &= h_1 + h_2 + m_2 r_2^2 + m_3(l_2^2 + r_3^2) + m_2 l_1 r_2 \cos\theta_2 \\
&\quad + (m_2 l_1 + 2m_3 r_3) l_2 \cos\theta_3 + m_3 l_1 r_3 \cos(\theta_2 + \theta_3) \\
M(1,3) &= h_3 + m_3 r_3^2 + m_3 l_2 r_3 \cos\theta_3 + m_3 l_1 r_3 \cos(\theta_2 + \theta_3) \\
M(2,1) &= M(1,2) \\
M(2,2) &= h_1 + h_2 + m_2 r_2^2 + m_3(l_2^2 + r_3^2) + 2m_3 l_2 r_3 \cos\theta_3 \\
M(2,3) &= m_3 l_2 r_3 \cos(\theta_1 + \theta_2) \\
M(3,1) &= M(1,3) \\
M(3,2) &= M(2,3) \\
M(3,3) &= h_3 + m_3 r_3^2 \\
C(1) &= (m_2 r_2 + m_3 l_2) l_1 (2\dot{\theta}_1 + \dot{\theta}_2)\dot{\theta}_2 \sin\theta_2 \\
&\quad + m_3 l_2 r_3 (2\dot{\theta}_1 + 2\dot{\theta}_2 + \dot{\theta}_3)\dot{\theta}_3 \sin\theta_3 \\
&\quad + m_3 l_1 r_3 (2\dot{\theta}_1 + \dot{\theta}_2 + \dot{\theta}_3)(\dot{\theta}_2 + \dot{\theta}_3) \sin(\theta_2 + \theta_3) \\
C(2) &= (m_2 r_2 + m_3 l_2) l_1 \dot{\theta}_1^2 \sin\theta_2 + m_3 l_1 r_3 \dot{\theta}_1^2 \sin(\theta_2 + \theta_3) \\
&\quad + m_3 l_1 r_3 (2\dot{\theta}_1 + 2\dot{\theta}_2 + \dot{\theta}_3)\dot{\theta}_3 \sin\theta_3 \\
C(3) &= m_3 l_1 r_3 \dot{\theta}_1^2 \sin(\theta_2 + \theta_3) + m_3 l_2 r_3 (\dot{\theta}_1 + \dot{\theta}_2)^2 \sin\theta_3 \\
G(1) &= (m_1 r_1 + (m_2 + m_3) l_1) g \sin\theta_1 \\
G(2) &= (m_2 r_2 + m_3 l_2) g \sin\theta_2 \\
G(3) &= m_3 r_3 g \sin\theta_3 \\
W(1) &= (m_1 r_1 + (m_2 + m_3) l_1) \ddot{D} \cos\theta_1 \\
W(2) &= (m_2 r_2 + m_3 l_2) \ddot{D} \cos\theta_2 \\
W(3) &= m_3 r_3 \ddot{D} \cos\theta_3
\end{aligned}$$

B Parameter values used in the base FRIPID scheduled control simulation

$$\mathbf{G}_{\mathrm{k}}^{(1)} = \begin{bmatrix} 91 & -60 & 26 \\ -24 & 25 & -8 \\ 20 & -12 & 10 \end{bmatrix}, \quad \mathbf{G}_{\mathrm{k}}^{(2)} = \begin{bmatrix} 60 & -90 & 32 \\ -7 & 25 & -4 \\ -7 & -55 & 8 \end{bmatrix},$$

$$\mathbf{I}_{1}^{(1)} = \begin{bmatrix} 470 & -220 & 164 \\ -46 & 200 & -17 \\ 200 & -113 & 125 \end{bmatrix},$$

$$\mathbf{I}_{1}^{(2)} = \begin{bmatrix} 503 & -286 & 176 \\ -60 & 170 & 0 \\ 212 & -113 & 125 \end{bmatrix}, \quad \mathbf{I}_2 = \begin{bmatrix} 60 & 0 & 0 \\ 0 & 60 & 0 \\ 0 & 0 & 60 \end{bmatrix},$$

$$\mathbf{I}_a = \begin{bmatrix} 0.1 & 0 & 0 \\ 0 & 0.1 & 0 \\ 0 & 0 & 0.1 \end{bmatrix},$$

$$\mathbf{I}_\tau = \begin{bmatrix} 0.07 & 0 & 0 \\ 0 & 0.01 & 0 \\ 0 & 0 & 0.16 \end{bmatrix}, \quad \mathbf{F}_2 = \begin{bmatrix} 0.65 & 0 & 0 \\ 0 & 0.65 & 0 \\ 0 & 0 & 0.65 \end{bmatrix},$$

$$\mathbf{MC} = \begin{bmatrix} 0.1 & 0 & 0 \\ 0 & 0.1 & 0 \\ 0 & 0 & 0.1 \end{bmatrix},$$

$$\mathbf{CA} = \begin{bmatrix} 0.32 & 0 & 0 \\ 0 & 0.04 & 0 \\ 0 & 0 & 0 \end{bmatrix}.$$

References

Allen GI, Tsukahara N (1974) Cerebrocerebellar communication systems. Physiol Rev 54:957–1006

Allum JH, Honegger F (1992) A postural model of balance-correcting movement strategies. J Vestib Res 2(4):323–347

Ayaso O et al (2002) Coarse gain recurrent integrator model for sensorimotor cortical command generation. In: Proceedings of the American control conference, Anchorage, AK

Bloedel JR, Courville J (1981) Cerebellar afferent systems. In: Bookhart JM, Mountcastle VB, Brooks VB, Geiger SR (eds) Handbook of physiology: The nervous system II, Sect I, vol II; Motor control, part 2. American Physiological Society, Bethesda, MD, pp 735–829

Braitenberg V (1967) Is the cerebellar cortex a biological clock in the millisecond range? Prog Brain Res 25:334–346

Brand RA et al (1986) The sensitivity of muscle force predictions to changes in physiological cross-sectional area. J Biomech 8:589–596

Brindley GS (1969) The use made by the cerebellum of the information that it receives from sense organs. Int Brain Res Org Bull 3:80

Brodal A (1981) Neurological anatomy in relation to clinical medicine. Oxford University Press, New York

Delp SL et al (1999) Variation of rotation moment arms with hip flexion. J Biomech 32:493–501

Diener HC, Dichgans J (1992) Pathophysiology of cerebellar ataxia. Mov Disord 7(2):95–109

Eccles JC et al (1967) The cerebellum as a neuronal machine. Springer, Berlin Heidelberg New York

Eccles JC et al (1974a) Temporal patterns of responses of interpositus neurons to peripheral afferent stimulation. J Neurophysiol 37:1427–1437

Eccles JC et al (1974b) Patterns of convergence onto interpositus neurons from peripheral afferents. J Neurophysiol 37:1438–1448

Feldman AG (1986) Once more on the equilibrium-point hypothesis (lambda model) for motor control. J Mot Behav 18(1):17–54

Flash T (1987) The control of hand equilibrium trajectories in multi-joint arm movements. Biol Cybern 57:257–274

Franklin GF et al (1994) Feedback control of dynamic systems, 3rd edn. Addison-Wesley, Reading, MA

Fuglevand AJ, Winter DA (1993) Models of recruitment and rate coding organization in motor-unit pools. J Neurophysiol 70(6):2470–2488

Fujita K, Sato H (1998) Intrinsic viscoelasticity of ankle joint during standing. In: Proceedings of the 20th annual international conference of the IEEE engineering in medicine and biology society, 20(5):2343–2345

Goodwin GC, Sin KS (1984) Adaptive filtering prediction and control. Prentice-Hall, Englewood Cliffs, NJ

Hallett M et al (1975) EMG analysis of stereotyped voluntary movements in man. J Neurol Neurosurg Psychiatry 38:1154–1162

Hasan Z (1983) A model of spindle afferent response to muscle stretch. J Neurophysiol 49(4):989–1006

Hemami H, Katbab A (1982) Constrained inverted pendulum model of evaluating upright stability. J Dyn Meas Syst Control 104:343–349

Henry SM et al (1998) Control of stance during lateral and anterior/posterior surface translations. IEEE Trans Rehabil Eng 6(1):32–42

Horak FB, Nashner LM (1986) Central programming of postural movements: adaptation to altered support-surface configurations. J Neurophysiol 55(6):1369–1381

Horak FB, Diener HC (1994) Cerebellar control of postural scaling and central set in stance. J Neurophysiol 72(2):479–493

Hore J, Flament D (1986) Evidence that a disordered servo-like mechanism contributes to tremor in movements during cerebellar dysfunction. J Neurophysiol 56:123–136

Hore J, Vilis T (1984) A cerebellar-dependent efference copy mechanism for generating appropriate muscle responses to limb perturbations. In: Bloedel JR, Dichgans J, Precht W (eds) Cerebellar functions. Springer, Berlin Heidelberg New York, pp 24–35

Hore J, et al (1976) Responses of cortical neurons (areas 3a and 4) to ramp stretch of hindlimb muscles in the baboon. J Neurophysiol 39:484–500

Ito M (1972) Neural design of the cerebellar motor control system. Brain Res 40:81–84

Ito M (1984) The cerebellum and neural control. Raven, New York

Ito M (1990) A new physiological concept on cerebellum. Rev Neurol Paris 146(10):564–569

Ito M (1997) Cerebellar microcomplexes. In: Schmahmann JD (ed) The cerebellum and cognition, vol 41. Academic, pp 475–487

Jo S (2002) A model of cerebellum-mediated long-loop control of upright balance. In: Proceedings of the 32nd annual meeting of the Society for Neuroscience, Orlando, FL

Johansson R et al (1988) Identification of human postural dynamics. IEEE Trans Biomed Eng 35(10):858–869

Johnson MTV, Ebner TJ (2000) Processing of multiple kinematic signals in the cerebellum and motor cortices. Brain Res Rev 33:155–168

Katayama M, Kawato M (1993) Virtual trajectory and stiffness ellipse during multijoint arm movement predicted by neural inverse models. Biol Cybern 69:353–362

Kettner RE et al (1997) Prediction of complex two-dimensional trajectories by a cerbellar model of smooth pursuit eye movement. J Neurophysiol 77:2115–2130

Kuo A (1995) An optimal control model for analyzing human postural balance. IEEE Trans Biomed Eng 42(1):87–101

Lacquaniti F, Soechting JF (1986) Simulation studies on the control of posture and movement in a multi-jointed limb. Biol Cybern 54:367–378

Leigh JR, Zee DS (1991) The neurology of eye movements. In: Plum F et al (eds) Contemporary neurology series, 2nd edn. FA Davis, Philadelphia, p 402

Li C-SR et al (2001) Neuronal correlates of motor performance and motor learning in primary motor cortex of monkeys adapting to an external force field. Neuron 30:593–607

Mann MD (1973) Clarke's column and the dorsal spinocerebellar tract: a review. Brain Behav Evol 7:34–83

Martin TA et al (1996) Throwing while looking through prisms: I. Focal olivocerebellar lesions impair adaptation. Brain 119:1183–1198

Massaquoi SG (1999) Modelling the function of the cerebellum in scheduled linear servo control of simple horizontal planar arm movements. PhD thesis Department of Electrical Engineering and Computer Science, MIT, Cambridge, MA, p 240

Massaquoi SG, Hallett M (1997) Ataxia and other cerebellar syndromes. In: Jankovic J, Tolosa E (eds) Parkinson's disease and movement disorders -3. Williams and Wilkins, Baltimore

Massaquoi SG, Hallett M (1998) Ataxia and other cerebellar syndromes. In: Jankovic J, Tolosa E (eds) Parkinson's disease and movement disorders. Williams and Wilkins, Baltimore, pp 523–686

Massaquoi SG, Slotine J-JE (1996) The intermediate cerebellum may function as a wave-variable processor. Neurosci Lett 215:60–64

Massaquoi SG, Topka H (2002) Models of cerebellar function. In: Pandolfo M, Manto M (eds) The cerebellum and its disorders. Cambridge University Press, Cambridge, pp 69–94

Miall RC et al (1993) Is the cerebellum a Smith predictor? J Mot Behav 25:1993

Nashner LM, Black FO, Wall C (1982) Adaptation to altered support and visual conditions during stance: patients with vestibular deficits. J Neurosci 2(5):536–544

Nashner LM, McCollum G (1985) The organization of human postural movements: a formal basis and experimental synthesis. Behav Brain Sci 8(1):135–150

Niemeyer G (1996) Using wave variables in time delayed force reflecting teleoperation. Aeronautics and astronautics. PhD thesis, MIT, Cambridge, MA

Ogihara N, Yanazaki N (2001) Generation of human bipedal locomotion by a bio-mimetic neuro-musculo-skeletal model. Biol Cybern 84:1–11

Osborn CE, Poppele RE (1992) Parallel distributed network characteristics of the DSCT. J Neurophysiol 68(4):1100–1112

Oscarsson O (1965) Functional organization of the spino- and cuneocerebellar tracts. Phys Rev 45:495–522

Oscarsson O (1979) Functional units of the cerebellum-sagittal zones and microzones. Trends Neurosci 2:143–145

Park S et al (2004) Postural feedback responses scale with biomechanical constraints in human standing. Exp Brain Res 154:417–427

Paulin MG (1993b) A model for the role of the cerebellum in motor control. Hum Mov Sci 12:5–16

Paulin MG (1997) Neural representations of moving systems. In: Schmahmann JD (ed) The cerebellum and cognition, vol 41. Academic, San Diego, pp 515–533

Peterka R (2001) Sensorimotor integration in human postural control. J Neurophysiol 88:1097–1118

Peterka R (2003) Simplifying the complexities of maintaining balance. IEEE Eng Med Biol Mag 22(2):63–68

Rosenthal NP et al (1970) Frequency analysis of stretch reflex and its main subsystems in triceps surae muscles of the cat. J Neurophyisol 33:713–749

Runge CF et al (1999) Ankle and hip postural strategies defined by joint torques. Gait Posture 10:161–170

Song J et al (1999) A simpified hybrid force/position controller method for the walking robots. Robotica 17:583–589

Spagele T et al (1999) Modelling, simulation and optimisation of a human vertical jump. J Biomech 32(5):521–530

Thach WT et al (1992a) The cerebellum and the adaptive coordination of movement. Annu Rev of Neurosci 15:403–442

Thach WT, et al (1992) Cerebellar output: multiple maps and modes of control in movement coordination. In: Llinas R, Sotelo C (eds) The cerebellum revisited. Springer, Berlin Heidelberg New York, p 283–300

Tremblay L et al (1998) Modifications of reward expectation-related neuronal activity during learning in primate striatum. J Neurophysiol. 80:964–977

Uno Y et al (1989) Formation and control of optimal trajectory in human multijoint arm movement. Biol Cybern 61:89–101

Van der Kooij H et al (1999) A multisensory integration model of human stance control. Biol Cybern 80:299–308

Winter DA (1990) Biomechanics and motor control of human movement, 2nd edn. Wiley, New York

Winters JM (1995) How detailed should muscle models be to understand multi-joint movement coordination? Hum Mov Sci 14:401–442

Wolpert DM et al (1995) An internal model for sensorimotor integration. Science 269:1880–1882

Wolpert DM et al (1998) Internal models in the cerebellum. Trend Cog Sci 2(9):338–347